ELSEVIER

Journal of Nuclear Materials 266–269 (1999) 1290–1295

journal of nuclear materials

Self-consistent impurity modeling in the Frascati Tokamak Upgrade

R. Zanino [a,*], C. Ferro [b], M. Frassinesi [a], M. Leigheb [b]

[a] *Dipartimento di Energetica, Politecnico, 24 c. Duca degli Abruzzi, I-10129 Torino, Italy*
[b] *Associazione EURATOM-ENEA, 00044 Frascati, Italy*

Abstract

SCOUT – a simple but self-consistent impurity model [1–4] – is used to describe impurity production and transport in the Frascati Tokamak Upgrade (FTU) operated with a molybdenum alloy (TZM) poloidal or segmented toroidal limiter. The values of main plasma impurity concentration parameter Z_{eff}, radiated power fraction $F_{\text{P}} \equiv P_{\text{rad}}/P_{\text{in}}$, and edge plasma density and temperature are computed and compared with measurements. Good agreement between model and experiment is found for medium to high plasma densities while at the lowest density Z_{eff} and F_{P} are typically underestimated and overestimated respectively.

Keywords: Impurities; Impurity transport; Modeling; FTU

1. Introduction

Impurities constitute one of the major problems of tokamak operation. Although divertors are presently the selected choice for plasma-wall interaction control in a tokamak reactor, clean plasmas have been obtained also in high-field, high-density limiter machines [5], thanks, among other reasons, to the screening action of the scrape-off layer (SOL). The increasing interest [6] for plasma facing components based on high-Z materials, e.g., Mo and W, becomes particularly relevant in this context.

In recent years a simple but self-consistent impurity model for limiter tokamaks – SCOUT – has been developed [1–3]. The model was validated [4] showing good agreement against experimental data of the Frascati Tokamak Upgrade (FTU) [5], operated with a poloidal Inconel (i.e., mainly Ni) limiter. Very recently the model has also been applied to a preliminary study of radiated power fraction $F_{\text{P}} \equiv P_{\text{rad}}/P_{\text{in}}$ and main plasma impurity concentration parameter Z_{eff} in Ignitor, for different limiter/first wall materials [7].

The SCOUT code was to our knowledge the first attempt taking impurity transport self-consistently into account both in the main plasma and in the SOL of a limiter tokamak. The SOL treatment was inspired by the LIM code of Stangeby [8], which had a more detailed Monte-Carlo treatment of the 2-D dynamics of the various impurity stages in the proximity of the limiter but no self-consistency. Subsequently, other similar self-consistent models were developed [9] and applied to the limiter configuration, including more detailed parallel dynamics but without taking accurately into account the limiter geometry. Very recently, finally, complex multi-fluid models have been developed (see, e.g., [10]), self-consistently coupling a 1-D treatment of the main plasma with a 2-D treatment of the divertor SOL. However, limiter plasma modeling has some qualitative differences with respect to the case of a divertor, which can partly justify the use of a simple model as done in SCOUT. Main plasma proximity to the limiter supports the assumption of contamination by neutral impurities only, with a reduced role of parallel dynamics. Modeling with sophisticated 2-D plasma codes, as done routinely for divertors, is very difficult because the magnetic field lines reach the limiter surface at angles varying continuously from zero to finite values, changing the sheath structure and resulting in not well defined boundary conditions.

* Corresponding author. Tel:. +39-011 564 4490; fax: +39-011 564 4499; e-mail: zanino@alphaz.polito.it.

0022-3115/99/$ – see front matter
PII: S0022-3115(98)00634-5

Here we present an extension of the SCOUT model to the segmented toroidal limiter geometry. The code is validated against data obtained in FTU with two different molybdenum alloy (TZM) limiters: a poloidal one and the present segmented toroidal one. The values of $Z_{\rm eff}$, $F_{\rm P}$, edge plasma density and temperature, are computed and compared with measurements, assuming Mo is the only impurity species in the plasma.

2. The Frascati Tokamak Upgrade (FTU)

FTU is a high toroidal field tokamak with major radius $R = 0.935$ m, minor radius $a = 0.295$ m, toroidal field $B_{\rm T} = 3.8$–7.8 T. FTU is characterized by a high average ohmic power density (1.5 MW/m^3), and a wide range of main plasma parameters [line averaged density $\bar{n}_{\rm e} \sim (0.2$–$2) \times 10^{20}$ m^{-3}, plasma current $I_{\rm p} = 0.3$–1.0 MA]. Plasma heating, full current drive and shear reversal with lower hybrid (LH), electron cyclotron and ion Bernstein radio-frequency have been the dominant scientific program so far.

The vacuum chamber is made of stainless steel AISI 304. A number of experimental campaigns were carried out with a poloidal limiter and devoted to studying the plasma characteristics when the limiter material is changed from the usual Inconel to molybdenum and tungsten. The vacuum chamber was modified afterwards, and since 1996 FTU operates with a large-area toroidal limiter (see, e.g., http://efrosf.frascati.enea.it/FTU). The limiter is formed of 12 sectors. Each sector consists of a stainless steel structure supporting 30 TZM tiles and covering a poloidal angle of about 70° on the inboard side of the vacuum vessel.

3. Numerical model

3.1. Brief overview of the SCOUT code

The SCOUT code [1–3] implements a self-consistent model for impurity production and transport, coupling main plasma and SOL according to a scheme which is summarized in Fig. 1. Sputtering at the limiter, with a production rate depending ultimately on the plasma temperature $T_{\rm w}$ in front of the solid, produces impurities. A fraction ε of them is ionized in the SOL and is brought back to the limiter by hydrodynamic friction. This fraction, the so-called screening efficiency, is computed taking carefully into account the plasma/wall geometry. (This care is particularly important for heavier impurities, characterized by shorter first ionization mean free path $\lambda_{\rm iZ}$. For instance, for plasma density 10^{19} m^{-3} and temperature 25 eV, $\lambda_{\rm iZ} \sim 2.9$ mm for Mo, 3.5 mm for Ni and 25 mm for C, respectively. These values can be compared with typical distances $\sigma \sim$ O (mm) to be

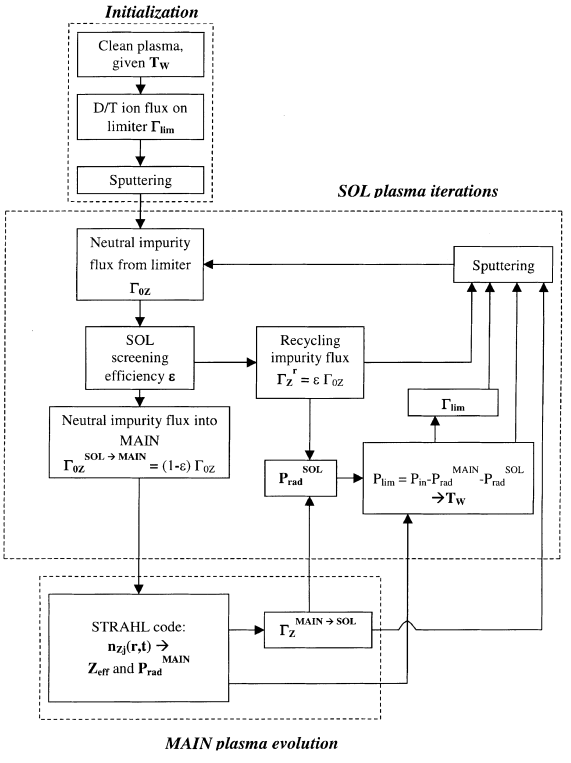

Fig. 1. Simplified flowchart of the SCOUT code.

traveled by the neutral impurity between limiter and LCMS in the case of FTU.) The remaining fraction $(1 - \varepsilon)$ is the time dependent neutral impurity influx $\Gamma_{0Z}^{\rm SOL\to MAIN}$ from SOL to main plasma. The latter drives the time evolution (1-D convection–diffusion) of the density n_{Zj} of each ionization stage of a single impurity species in the main plasma, which is modeled with a version of the STRAHL code [11]. The radial profiles of n_{Zj} computed at each time step determine $Z_{\rm eff}$ and the radiated power $P_{\rm rad}^{\rm MAIN}$. The cycle is then closed computing an updated value of $T_{\rm w}$ from the power conducted and convected to the limiter, $P_{\rm lim} = P_{\rm in} - P_{\rm rad}^{\rm MAIN} - P_{\rm rad}^{\rm SOL}$, for a given constant input power $P_{\rm in}$.

While the impurity profiles in the main plasma evolve on the slow radial transport time scale, the impurities in the SOL undergo faster transients on the sound time scale. This justifies the approximation used in SCOUT of an iterative treatment for the SOL plasma, repeated at each time step of the evolution in the main plasma. For the sake of model simplicity and because here we are using the code in an interpretative mode for comparison with experimental results, the electron density and temperature profiles in the main plasma are assumed at steady state. [This becomes a problem if, at some time during the transient, $P_{\rm rad}^{\rm MAIN} > P_{\rm in}$ (see below).] These profiles are parameterized using only experimental peak and average values as reported in Tables 1 and 2.

In the STRAHL portion of the code the minor radius of the main plasma is discretized with a grid, which is strongly non-uniform and refined near the SOL in order to resolve the first ionization source and the low ionization stages. This notwithstanding, the spatial convergence of STRAHL at high plasma densities and with high Z impurities can only be guaranteed if many points, at least ~500, say, are used [4]. The very short first ionization mean free path, which obtains in that case, results in fact in a very narrow source concentrated near the plasma edge. Adaptive time stepping is needed in order to avoid large negative impurity densities during the transient, which leads to the steady state of interest for us here [4].

3.2. Model of the segmented toroidal limiter

A single sector of the toroidal limiter has been modeled. The poloidal profile (identified by a set of 61 points) is characterized by being tangent to the last closed magnetic surface (LCMS) up to an elevation of about 0.09 m above/below the midplane. On each horizontal plane the toroidal profile of the sector is circular and it reaches on the midplane a maximum distance of about 0.003 m from the LCMS. [This slight eccentricity with respect to the plasma is sufficient to give a computed ratio of particle load received by the limiter (toroidally/poloidally) of about 4.]

One quadrant of the sector surface is discretized with rectangular elements using 10 points in the toroidal direction (a finer resolution proved not to be necessary). We assume that sputtered impurities leave each of these elements along rays normal to the limiter surface. The global screening efficiency is then computed starting from the local ionization probability along each ray [1], and integrating over the quadrant.

In the model, both particle load and conductive–convective energy loads reach the limiter along magnetic field lines, so that the tangent portion of the limiter does only receive a fraction of the isotropic radiative load. Shadowing effects [12] are not taken into account.

4. Results

The description of the impurities in the main plasma requires the assumption of a transport model. In the version of the STRAHL code coupled [3] to our SOL model each ionization stage has given (anomalous) diffusion coefficient $D(r)$ and inward pinch speed $V(r)$, while neoclassical transport is not implemented. (Inclusion of neoclassical transport in the main plasma model could, indeed, be particularly important for high Z impurities in high density plasmas, because of their high collisionality, but it is beyond the scope of the present work.)

The diffusion coefficient profiles are assumed to stay constant at $D(0)$ until at $(r/a) = 0.9$ they start growing linearly to $D(a) = 0.8$ m^2/s. The inward pinch speed grows linearly from 0 to $V(a)$. The main plasma transport scenarios used in the present study are:

- α [$D(0) = 0.4$ m^2/s, $V(a) = 6$ m/s] the reference scenario [13] for the poloidal limiter,
- β [$D(0) = 0.7$ m^2/s, $v(a) = 5$ m/s] the reference scenario [14] for the toroidal limiter,
- γ [$D(0) = 0.1$ m^2/s, $v(a) = 8$ m/s] an ad hoc "high-confinement" scenario mainly used to test for both cases the influence of transport coefficients in the main plasma on impurity parameters.

Concentric circular magnetic surfaces are assumed for both the poloidal and the toroidal limiter plasmas.

The model is run to a steady state, which is typically reached in ~0.5 s (see below for exceptions). The steady state results are then compared with the experiment.

4.1. Poloidal limiter

We have analyzed with the SCOUT code 5 FTU discharges with a poloidal TZM limiter. The structure of the limiter and the way it is modeled in SCOUT were already discussed in Ref. [1] and will not be repeated here. The input plasma parameters for these simulations have been obtained from the public domain database described in Ref. [15] and the major characteristics of

Table 1
Data for poloidal limiter shots [13]

Shot number	7304	7334	7312	7353	7355
$\bar{n}_e$ (10^{20} m^{-3})	0.55	0.88	1.39	1.95	2.63
$\langle n_e \rangle$ (10^{20} m^{-3})	0.40	0.76	1.03	1.57	2.08
$n_e(0)$ (10^{20} m^{-3})	0.92	1.13	2.25	2.8	3.89
$\langle T_e \rangle$ (keV)	0.52	0.36	0.28	0.30	0.27
$T_e(0)$ (keV)	1.80	1.37	1.06	0.94	0.84
P_{in} (MW)	0.56	0.64	0.75	1.28	1.34
B_T (T)	5.74	5.72	5.74	5.74	5.74
I_p (MA)	0.51	0.50	0.49	0.68	0.68

Table 2
Data for toroidal limiter shots

Shot number	12691	13279	12486	13295
$\bar{n}_e$ (10^{20} m^{-3})	0.5	0.8	1.2	1.5
$\langle n_e \rangle$ (10^{20} m^{-3})	0.29	0.62	0.90	1.1
$n_e(0)$ (10^{20}m^{-3})	0.97	1.25	1.85	1.7
$\langle T_e \rangle$ (keV)	0.42	0.46	0.34	0.56
$T_e(0)$ (keV)	2.0	1.7	1.35	1.4
P_{in} (MW)	0.38	0.6	0.59	1.2
B_T (T)	5.09	6.0	5.71	6.0
I_p (MA)	0.36	0.5	0.5	0.8

these shots have been summarized in Table 1. They scan between $\bar{n}_e \sim 0.5 \times 10^{20}$ and $\bar{n}_e \sim 2.5 \times 10^{20}$ m^{-3}, and as such can be considered representative of the operating space of the machine.

We see that a good agreement is obtained at medium to high $\bar{n}_e$ both for Z_{eff} [Fig. 2(a)] and for F_P [Fig. 2(b)]. We notice also that the agreement in F_P generally improves when going from the reference α scenario to the ad hoc γ scenario.

The drop in F_P for shot 7334 is probably due in the model to a combined effect. A relatively high edge density obtains for this shot, $n(a) \sim 2 \times 10^{19}$ m^{-3}, if compared to that of shot 7312, for which $n(a) \sim 1 \times 10^{19}$ m^{-3}. This is due to the fact that $n(a)$ is computed imposing the continuity of the particle flux through the LCMS, and the profile $n_e(r)$ is significantly more peaked in shot 7312 than in shot 7334 (Table 1). The higher $n(a)$ gives improved screening and, together with the lower $n(0)$, lower radiated power in shot 7334.

At the lowest $\bar{n}_e$ (shot 7304) we notice that the model underestimates Z_{eff}, while F_P is overestimated. The reason for this discrepancy is not clear. Scenario γ would in principle lead to a higher Z_{eff} but it simultaneously gives an increase of the radiated power, until at some point during the simulation $P_{rad}^{MAIN} > P_{in}$. This 'thermal collapse' forces the simulation to stop because the main plasma density and temperature profiles are given once and for all, as seen above. The inclusion in the model of a simplified energy equation as in Ref. [9] would allow the simulation to proceed but, although this strategy is useful in a predictive computation, it is doubtful that it can be practical when using the code in an interpretative mode as done here.

4.2. Segmented toroidal limiter

For this case we have analyzed 4 discharges, with characteristics summarized in Table 2. At medium to high $\bar{n}_e$ the agreement between model and experiment is again good both concerning Z_{eff} [Fig. 3(a)] and F_P [Fig. 3(b)]. At the lowest $\bar{n}_e$, the trend seen above in the poloidal case to underestimate Z_{eff}, simultaneously overestimating F_P, is repeated here. Also similarly to what seen before, the ad hoc γ scenario does not allow

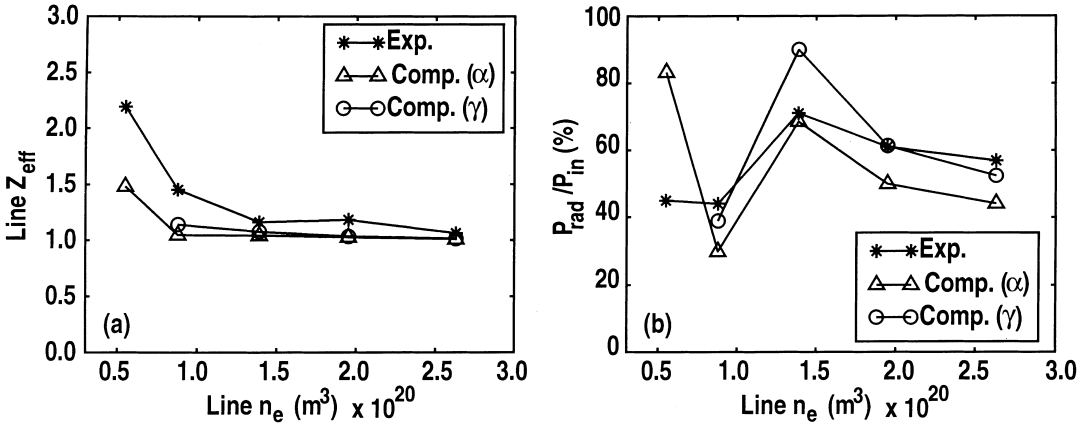

Fig. 2. Comparison between computed and experimental values of line averaged Z_{eff} (a) and radiated power fraction F_P (b) vs. line averaged electron density $\bar{n}_e$, in the case of the poloidal Mo limiter in FTU. Measured values (*), computed values for α transport scenario (triangles), computed values for γ transport scenario (circles).

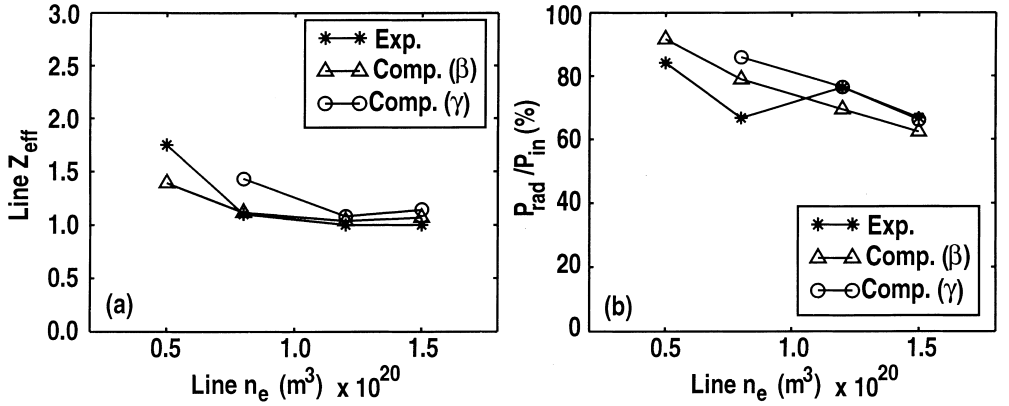

Fig. 3. Comparison between computed and experimental values of line averaged $Z_{\rm eff}$ (a) and radiated power fraction $F_{\rm P}$ (b) vs. line averaged electron density $\bar{n}_{\rm e}$, in the case of the toroidal Mo limiter in FTU. Measured values (*), computed values for β transport scenario (triangles), computed values for transport scenario (circles).

the code to reach a steady state at the lowest $\bar{n}_{\rm e}$ because at some instant during the computed transient $P_{\rm rad}^{\rm MAIN}$ becomes larger than $P_{\rm in}$.

In the case of the toroidal limiter we also have, for 2 of the discharges analyzed, experimental measurements of plasma density and temperature at the LCMS from reciprocating Langmuir probes [14]. These are compared with the results of the simulation in Table 3. We notice that the experimental values always fall, independently of the transport scenario, between the computed values at the limiter (w suffixes) and at the midplane far from the limiter, $n(a)$ and $T(a)$. This indicates good agreement between model and experiment even concerning local quantities, as opposed to global ones considered so far. The existence of parallel gradients in the SOL, as predicted by the SCOUT code (Table 3) is also experimentally confirmed and associated to long connection lengths [15].

As a byproduct of the present simulations the distribution of the power load on the limiter surface was computed under the assumption of isotropic radiation and anisotropic conduction–convection along magnetic field lines. For instance, with the reference β scenario we used an energy SOL length $\lambda_E = (4/7)\lambda_n$, and the density SOL length λ_n as estimated [typically O(cm)] by the model [2]. The estimate for λ_E comes from assuming that the parallel energy flux is proportional to $nc_sT \sim nT^{3/2}$ and that the temperature decay length in the SOL $\sim 2\lambda_n$. We estimate peak power loads below 2MW/m^2 and peaking factors $\sim$4, without taking into account the shadowing effect between adjacent sectors. This result differs from those of [12] where, however, the poloidal shape of the limiter was rather different from the actual one, which is used here. Unfortunately, no experimental measurement of the power load is available at present.

5. Conclusions and perspective

The SCOUT code [1–4] has been extended to treat a segmented toroidal limiter geometry and validated with

Table 3
Edge quantities (toroidal limiter)

Shot number		12691	13279	12486	13295
$n_{\rm e}^{\rm edge}$ (exp) (10^{19} m^{-3})		–	1.2	–	3.1
β	$n(a)$	0.29	1.36	1.87	3.62
	$n_{\rm w}$	0.16	0.88	1.28	2.60
γ	$n(a)$	[a]	1.32	1.84	3.60
	$n_{\rm w}$	[a]	0.94	1.35	2.66
$T_{\rm e}^{\rm edge}$ (exp) (eV)		–	22	–	28
β	T(a)	26.2	27.0	27.1	29.7
	$T_{\rm w}$	24.3	20.9	19.9	20.7
γ	T(a)	[a]	22.9	24.5	28.5
	$T_{\rm w}$	[a]	16.1	16.7	19.3

[a] Steady state not reached in this case.

molybdenum as the impurity species. Both poloidal and toroidal TZM limiter discharges in FTU have been simulated. Good agreement was found, for medium to high $\bar{n}_e$ ($\geqslant 1 \times 10^{20}$ m^{-3}), between computed and experimental Z_{eff}, radiated power fraction F_P, edge plasma densities and temperatures. At the lowest $\bar{n}_e$ considered here ($\sim 5 \times 10^{19}$ m^{-3}) – a regime, however, of less interest for us – Z_{eff} and F_P are typically underestimated and overestimated, respectively.

In perspective we plan to further validate the model against data from the C-Mod tokamak operated with a purely toroidal, vertically flat limiter coinciding with a portion of the inboard first wall, and to extend the study of impurities in the Ignitor project [7].

References

[1] C. Ferro, R. Zanino, J. Nucl. Mater. 196–198 (1992) 321.
[2] R. Zanino, C. Ferro, Contrib. Plasma. Phys. 34 (1994) 337.
[3] R. Zanino, C. Ferro, Europhys. Conf. Abstracts 18B (1994) 822.
[4] R. Zanino, C. Ferro, Contrib. Plasma. Phys. 36 (1996) 260.
[5] M.L. Apicella et al., Nucl. Fusion 37 (1997) 381.
[6] N. Noda, V. Philipps, R. Neu, J. Nucl. Mater. 241–243 (1997) 227.
[7] R. Zanino, C. Ferro, M. Frassinesi, presented at the 6th International Workshop on Plasma Edge Theory, Oxford, UK, 1997.
[8] P.C. Stangeby, C. Farrell, L. Wood, Contrib. Plasma. Phys. 28 (1988) 501.
[9] R. Zagorski, F. Romanelli, Contrib. Plasma. Phys. 36 (1996) 145.
[10] M. Fichtmueller et al., these Proceedings.
[11] K. Behringer, JET Report R(87)08, 1987.
[12] M. Ciotti, C. Ferro, G. Maddaluno, J. Nucl. Mater. 196–198 (1992) 725.
[13] L. Gabellieri, G. Mazzitelli, Europhys. Conf. Abstracts 19C (1995) 77.
[14] D. Pacella, M. Leigheb, M. Mattioli, Phys. Scripta 57 (1998) 265.
[15] S.M. Kaye et al., Nucl. Fusion 37 (1997) 1303.